21, rue d'Artois, F-75008 PARIS
http : //www.cigre.org

CIGRE US National Committee
2022 Grid of the Future Symposium

Enabling Distribution System to Participate in Secondary Frequency Regulation

J. THAPA, M. BENIDRIS, H. LIVANI
University of Nevada at Reno
USA

SUMMARY

Coordinated and optimal operation of distributed energy resources (DERs) can enable active distribution networks (ADNs) to contribute in grid services such as frequency regulation and control. Although the contribution of a single ADN in grid services may not be significant, when coordinated and stacked, contributions of multiple ADNs can provide grid services at scale. This paper proposes a secondary frequency regulation (SFR) scheme to optimally dispatch DERs when system operator (SO) sends a command to change the amount of power production from sources behind the substation. The optimization problem is formulated based on a linearized power flow model for unbalanced distribution networks---the linearized power flow model keeps the optimization problem tractable and guarantees the uniqueness of the solution with a high speed of computation, which is needed for SFR. To correct potential errors introduced by the linearized power flow model, the proposed scheme measures actual delivered power at the substation and corrects any mismatches between actual delivered power and the requested amount of power change. Also, the ZIP (impedance, current, and power) load model is used to improve the accuracy of response to SO commands. The proposed approach is demonstrated on the modified 33-node and IEEE 13-node distribution systems. The results show that the proposed approach accurately dispatches DERs to participate in secondary frequency regulation.

KEYWORDS

Linearized power flow, optimal dispatch, secondary frequency, unbalance distribution network

jitendrathapa@nevada.unr.edu

Nomenclature

$P_i^{\emptyset}, Q_i^{\emptyset}$	Active and reactive line flow from node i for phase Ø
$V_0^{\emptyset}, V_i^{\emptyset}$	Substation voltage as reference and voltage of node i for phase Ø
$P_{loss,i}^{\emptyset}, Q_{loss,i}^{\emptyset}$	Active and reactive loss on the line connected to node i for phase Ø
$P_{L,i}^{\emptyset}, Q_{L,i}^{\emptyset}$	Active and reactive load connected to node i on phase Ø
$X_i^{\emptyset}, R_i^{\emptyset}$	Line reactance and resistance from node i for phase Ø
N, N_{DER}	Number of nodes & Number of DERs
$\Delta P_{sys}, \Delta P_{subs}$	SO requested change of power & Power change at the substation
$P_{DER,j}, Q_{DER,j}$	Set points of power for jth DER
$P_{DER}^{min}, P_{DER}^{max}$	DER lower and upper active power bounds
θ	Power Factor Angle
$k_{p,1}, k_{q,1}$	Coefficients for constant impedance of active and reactive power of ZIP load
$k_{p,2}, k_{q,2}$	Coefficients for constant current of active and reactive power of ZIP load
$k_{p,3}, k_{q,3}$	Coefficients of constant power of active and reactive power of ZIP load

I. Introduction

Frequency regulation has been a challenge to system operators (SOs) due to high penetration of renewable energy sources. Traditionally, frequency imbalances are regulated using conventional synchronous generators through sequentially activating primary frequency control (local), automatic generation control (AGC), and spinning and non-spinning reserves. However, as penetration level of distributed energy resources (DERs) increases, contribution of spinning conventional synchronous generators may not be significant to restore frequency deviations. The fast dynamic response capability of DERs can be utilized to allow them to participate in frequency regulation [1] and help SOs gain more time to bring non-spinning units into service. However, due to being small and dispersed in comparison with synchronous generators, DERs cannot provide significant and attractive resources for SOs unless DERs are controlled and aggregated. Therefore, there is an urgent need to optimally operate and coordinate between different DERs in active distribution networks (ADNs) to participate in grid services such as frequency regulation.

Several approaches have been developed to utilize DERs in frequency regulation. In [2], a wind farm has been enabled to provide SFR through the use of model-based receding horizon control. A model predictive controller with a surrogate wind farm model has been presented in [3] to track a reference power signal generated by transmission system operators for SFR. The operation of a multitasking battery storage system for reducing grid peak loads, storing surplus photovoltaic energy, and providing secondary control reserve to restore the grid frequency to its nominal value has been presented in [4]. In [5], investigation of 5G-networked shipboard multi-microgrid for secondary load frequency control has been conducted. The work presented in [6] has proposed a strategy for coordinated operation of battery energy storage systems and wind power plant with variable generation to ensure frequency ancillary services including both primary and secondary frequency control. An experimental performance analysis has been conducted in [7] for wind farm participation in frequency regulation. Moreover, the experiment has demonstrated that the wind farm can regulate its active power to accurately track a varying active power target command. A secondary frequency control signal tracking method has been presented in [8] by combining plug-in-hybrid electric vehicles, controllable load, and a co-generation unit. The investigation of supplementary load frequency control on power system with high penetration of photovoltaic and wind power generation has been carried out in [9] using both EV and heat pump water heater as controllable loads. The work proposed in [10] has adopted a risk-averse multi-armed bandit learning technique to aggregate demand-side in order to provide reliable regulation for secondary frequency. In [11], a fuzzy logic battery control strategy based on area control error (ACE) and area regulation requirement (ARR) signals has been developed to enhance the SFR. Most of the existing studies has address SFR in microgrids and transmission system. Therefore, enabling the participation of ADNs for frequency regulation through the optimal operation of modern advanced distribution assets will be a valuable resource for SOs.

This paper proposes a SFR scheme through real-time optimal dispatch of DERs in unbalanced distribution networks. The significance of this work is to provide SOs with a new tool for SFR using distribution feeder's asset. This new tool will fill the gap between the time that conventional AGC resources are dispatched, and the spinning resources are requested to respond. The proposed approach involves the formulation of optimization algorithm through linearization of phase decoupled power flow equations for dispatching the command of the SO among the participating DERs, and simultaneously reducing the active loss of the distribution system. The injection of active power at the substation is observed at the starting and the end of each iteration to estimate and correct the error between requested power and delivered power. An iterative optimization is performed to minimize the mismatch if the error is beyond the threshold. In order to reduce the computational time and keep the optimization problem tractable, the problem formulation is modelled as a Linear Programming problem with linearized model of DERs, ZIP loads, and other components. The effectiveness of the proposed approach is demonstrated through several case-studies in IEEE standard unbalance distribution networks.

The remainder of the paper is organized as follows. Section II describes detailed linearized modelling of power flow and components in the distribution system. Section III describes formulation of the problem for calculating the amount of participation of each DERs through an optimization. Section IV provides the implementation results through several case studies on the modified 33-node and IEEE 13-node unbalanced distribution networks. Section V provides concluding remarks.

II. Power Flow and Component Modelling

A. Linearized Decoupled Three Phase Power Flow Modelling

Single Phase DistFlow equations [12] can be extended to formulate a phase-decoupled three-phase power flow model. Consider a portion of radial distribution network as shown in Fig. 1 for which three-phase AC power flow equations in DistFlow form can be written $\forall i = 1, \ldots, N$ as:

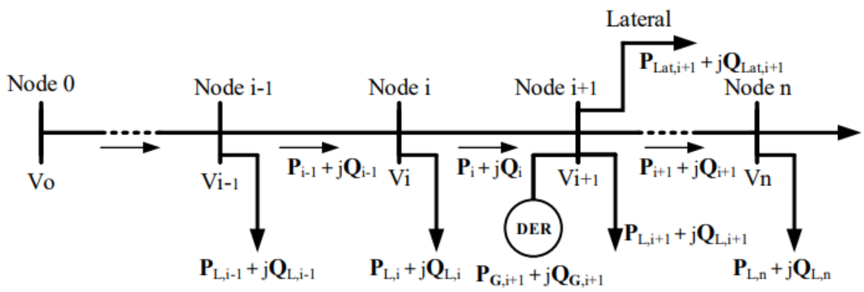

Fig. 1. Oneline Diagram of Radial Network

$$P_{i+1}^{\emptyset} = P_i^{\emptyset} - R_i^{\emptyset}\left(\frac{(P_i^{\emptyset})^2 + (Q_i^{\emptyset})^2}{(V_i^{\emptyset})^2}\right) - P_{L,i+1}^{\emptyset} - P_{Lat,i+1}^{\emptyset} + P_{G,i+1}^{\emptyset}, \forall i, \emptyset \tag{1}$$

$$Q_{i+1}^{\emptyset} = Q_i^{\emptyset} - X_i^{\emptyset}\left(\frac{(P_i^{\emptyset})^2 + (Q_i^{\emptyset})^2}{(V_i^{\emptyset})^2}\right) - Q_{L,i+1}^{\emptyset} - Q_{Lat,i+1}^{\emptyset} + Q_{G,i+1}^{\emptyset}, \forall i, \emptyset \tag{2}$$

$$V_{i+1}^{\emptyset^2} = V_i^{\emptyset^2} - 2\left(R_i^{\emptyset} P_i^{\emptyset} + X_i^{\emptyset} Q_i^{\emptyset}\right) + \left(R_i^{\emptyset^2} + X_i^{\emptyset^2}\right)\left(\frac{(P_i^{\emptyset})^2 + (Q_i^{\emptyset})^2}{(V_i^{\emptyset})^2}\right), \forall i, \emptyset \tag{3}$$

The quadratic terms in the active and reactive power flow equations represent branch losses because of which the equations are non-linear. The fully linearized DistFlow equation presented in [13] for each phase including the power loss term is formulated as follows,

$$P_{i+1} = P_i - P_{loss,i} - P_{L,i+1} - P_{Lat,i+1} + P_{G,i+1}, \forall i \tag{4}$$

$$Q_{i+1} = Q_i - Q_{loss,i} - Q_{L,i+1} - Q_{Lat,i+1} + Q_{G,i+1}, \forall i \tag{5}$$

$$V_{i+1} = V_i - \frac{R_i P_i + X_i Q_i}{V_0}, \forall i \quad (6)$$

$$P_{loss,i} = \sum_{j \in J_i} a_{i,j}(P_{i,j} - P_{i,j}^*) + \sum_{k \in K_i} b_{i,k}(Q_{i,k} - Q_{i,k}^*) \quad (7)$$

$$Q_{loss,i} = \sum_{j \in J_i} c_{i,j}(P_{i,j} - P_{i,j}^*) + \sum_{k \in K_i} d_{i,k}(Q_{i,k} - Q_{i,k}^*) \quad (8)$$

$$P_i = \sum_{j \in J_i}(P_{i,j} + P_{i,j}^*),\ Q_i = \sum_{k \in K_i}(Q_{i,j} + Q_{i,j}^*) \quad (9)$$

$$0 \le P_{i,j} \le P_i^j - P_i^{j-1}, \forall\, i,j \quad (10)$$

$$P_i^{j-1} - P_i^j \le P_{i,j}^* \le 0, \forall\, i,j \quad (11)$$

$$0 \le Q_{i,k} \le Q_i^k - Q_i^{k-1}, \forall\, i,k \quad (12)$$

$$Q_i^{k-1} - Q_i^k \le Q_{i,k}^* \le 0, \forall\, i,k \quad (13)$$

$$f_i(x) = \frac{R_i}{V_0^2}x^2,\ g_i(x) = \frac{X_i}{V_0^2}x^2; \forall i \quad (14)$$

$$a_{ij} = \frac{f_i(P_i^j) - f_i(P_i^{j-1})}{P_i^j - P_i^{j-1}}, \forall i,j \quad (15)$$

$$b_{ik} = \frac{f_i(Q_i^k) - f_i(Q_i^{k-1})}{Q_i^k - Q_i^{k-1}}, \forall i,k \quad (16)$$

$$c_{ij} = \frac{g_i(P_i^j) - g_i(P_i^{j-1})}{P_i^j - P_i^{j-1}}, \forall i,j \quad (17)$$

$$d_{ik} = \frac{g_i(Q_i^k) - g_i(Q_i^{k-1})}{Q_i^k - Q_i^{k-1}}, \forall i,k \quad (18)$$

Equations (4)-(6) shows how two adjacent buses are related in terms of line flows, and voltages. Equations (7) and (8) indicate the linear formulation of line losses. Equation (9) shows division of complex power variable into linear pieces. Equations (10)-(13) represent the bound of variables related to linear piece. The sign * indicates the reverse line flow variable. Equations (14)-(18) calculates the linear equation slope.

B. ZIP Load Modelling

Power system studies require simple and accurate mathematical models to approximate the characteristics of modern load behaviours. The most commonly used load model for both steady-state and dynamic studies is ZIP model that combines the constant impedance (Z), constant current (I) and constant power (P) characteristics of the load. The ZIP load model, also referred to as polynomial load model, represents the dependency of load on voltage magnitude using polynomial equation. Equations (19) and (20) describe the mathematical representation of ZIP load model for a load connected to node i on phase ∅.

$$P_{L,i}^{\emptyset} = P_{i,0}^{\emptyset}\left[k_{p,i}\left(\frac{V_i^{\emptyset}}{V_{nom}}\right)^2 + k_{p,2}\left(\frac{V_i^{\emptyset}}{V_{nom}}\right) + k_{p,3}\right], \forall i, \emptyset \quad (19)$$

$$Q_{L,i}^{\emptyset} = Q_{i,0}^{\emptyset}\left[k_{q,i}\left(\frac{V_i^{\emptyset}}{V_{nom}}\right)^2 + k_{q,2}\left(\frac{V_i^{\emptyset}}{V_{nom}}\right) + k_{q,3}\right], \forall i, \emptyset \quad (20)$$

where, $k_{p,1} + k_{p,2} + k_{p,3} = 1$, $k_{q,1} + k_{q,2} + k_{q,3} = 1$, and ($P_{i,0}^{\emptyset}$, $Q_{i,0}^{\emptyset}$) are load consumption per phase at nominal voltage V_{nom}. Equations (19) and (20) show the non-linear relationship between consumed power and the voltage at the respective node i. In order to adjust the ZIP load in the linearized power flow model, the quadratic voltage term should be linearized. As the per unit voltages of all the nodes are within 0.9 and 1.05, the quadratic term of the voltage at $V_{nom} = 1$ p.u. can be replaced by $V_i^2 = 2V_i - 1$

Substituting the value of V_i^2 in equations (19) and (20), we get,

$$P_{L,i}^{\emptyset} = P_{i,0}^{\emptyset}\left[\left(2k_{p,1}+k_{p,2}\right)\left(\frac{V_i^{\emptyset}}{V_{nom}}\right)+\left(k_{p,3}-k_{p,1}\right)\right], \forall i, \emptyset \quad (21)$$

$$Q_{L,i}^{\emptyset} = Q_{i,0}^{\emptyset}\left[\left(2k_{q,1}+k_{q,2}\right)\left(\frac{V_i^{\emptyset}}{V_{nom}}\right)+\left(k_{q,3}-k_{q,1}\right)\right], \forall i, \emptyset \quad (22)$$

Equations (21) and (22) represent the linearized modelling of the active and reactive component of ZIP load.

C. DER Modelling

Based on the output characteristics, two types of DERs are modelled, one is capable of dispatching both active and reactive power whereas the other one is modelled with power factor of 1, i.e., capable of providing active power only. These DERs are assumed to be operated and their reference power set-points are controlled based on Grid-Following mode. The generalized DERs model having both output characteristics is as follows,

$$0 \leq P_{DER,j} \leq P_{DER,j}^{max}, \forall j \in 1, \dots, N_{DER} \quad (23)$$

$$-\tan(\theta) \times P_{DER.j} \leq Q_{DER,j} \leq \tan(\theta) \times P_{DER,j}, \forall j \in 1, \dots, N_{DER} \quad (24)$$

III. Problem Formulation

A. Optimization Problem

The optimization problem is formulated viewing SFR can be solved through optimal and coordinated dispatch of distribution assets like distributed energy resources, and battery storage. So, the optimization problem is developed with loss minimization as an objective and simultaneously satisfying the exact increment or decrement of active power appealed by the SO in response to minimize the deviation in the frequency. When loss minimization is taken as an objective function, it indirectly maximizes the usage of DERs which in turn reduces the power supply from the grid to meet the total demand of the distribution system. Loss minimization and optimal dispatch for SFR is done simultaneously through this approach. The optimization problem is formulated as follows,

$$min \sum_{i=1}^{N-1} \sum_{j=1}^{\emptyset} R_i^{\emptyset}\left[\frac{(P_i^{\emptyset})^2+(Q_i^{\emptyset})^2}{(V_i^{\emptyset})^2}\right] \quad (25)$$

subjected to:

$$\Delta P_{sys} = \sum_{j=1}^{N_{DER}} \Delta P_{DER,j} + \Delta P_{loss} \quad (26)$$

$$V_{min}^{\emptyset} \leq V_i^{\emptyset} \leq V_{max}^{\emptyset}, \forall i \in 1, \dots, N \quad (27)$$

and equations. (4-18), (21-22), (23-24)

Equation (25) represents the objective function which is minimization of overall loss of the distribution system with DERs being re-dispatched for the purpose of frequency regulation. Constraint (26) describes the quantity of active power change appealed by the SO that should be satisfied by the combination of changes in active power output of DERs and the resulting change in network loss. Constraint (27) presents the lower and upper bound of voltage at each node. Equations (4-18) represent the power flow constraint as an equality constraint, (21-22) represents the equality constraints of ZIP loads, (23-24) presents the inequality constraints for the maximum and minimum limits of each participating DERs.

B. *Proposed Algorithm*

The proposed algorithm to optimally dispatch the DERs for SFR is shown in Fig. 2. The algorithm works in timeline between the response time of fast AGC resources and slow responding resources (spinning and non-spinning reserves) for frequency regulation. SO requests increase in DER'S generation for up-regulation and decrease in generation for down-regulation when there is a need to balance supply and demand in the system. The optimization scheme calculates the optimal set-points of DERs based on the requirement of increasing or decreasing the frequency with an objective of minimizing the loss and satisfying the SO's request. In this paper, full AC power flow model of the network is considered as a reference model to measure the power at the substation before and after re-dispatch of DERs obtained from our proposed algorithm. If the change of power at the substation is not equivalent to the quantity appealed by the SO, another round of optimization is performed to compensate the deficit or excess amount. Equation (28) represent the formula to calculate the absolute error.

$$|Error|\% = \frac{|\Delta P_{subs} - \Delta P_{sys}|}{\Delta P_{sys}} \times 100 \tag{28}$$

$$\Delta P_{sys} - \varepsilon \leq \Delta P_{subs} \leq \Delta P_{sys} + \varepsilon \tag{29}$$

Equation (29) represents the substation's power change after optimally dispatching the set-points DERs and should be equivalent to power appealed by the SO within a given tolerance. This bound is used as a stopping criterion for the iterative optimization algorithm. The second iteration is conducted by the optimizer for the corrective action. The number of iterations required to precisely dispatch the quantity of power appealed by the SO depends upon the accuracy of the linearized model.

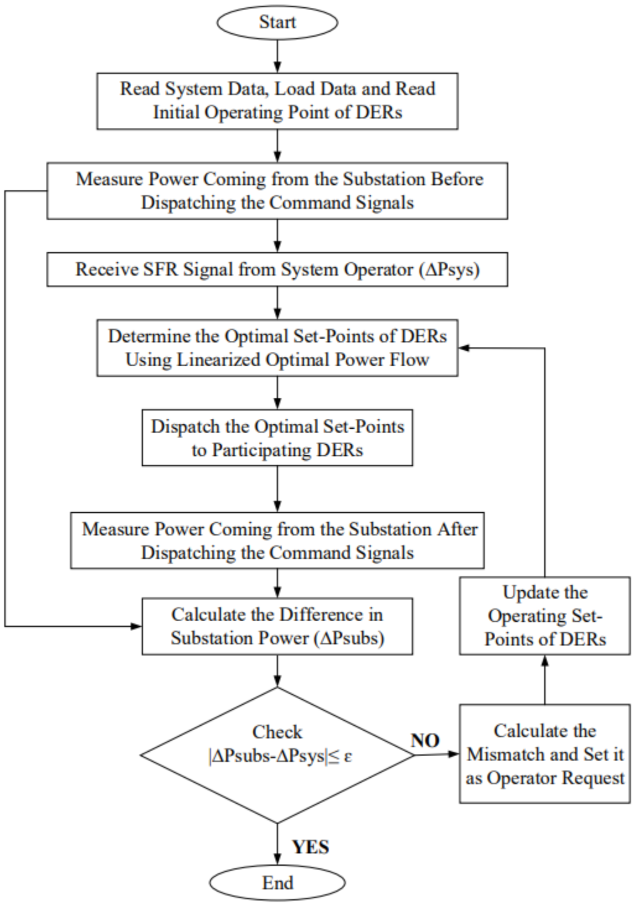

Fig. 2. Flowchart of Proposed Approach for SFR

IV. Case Studies and Results

This section shows several test cases to validate the accuracy and effectiveness of the proposed algorithm for SFR tested on 33-node and IEEE-13 node distribution networks.

A. Case Study on the Modified 33-node System

The modified 33-node system shown in Fig. 3 is used to demonstrate the effectiveness of the proposed approach. The data for impedance of the lines and base loads at each node of the system is taken from [14]. Loads on each node are modelled as a ZIP load with constant impedance, constant current and constant power coefficient as 0.4, 0.1 and 0.5 respectively. Three-phase power and voltage of 10 MVA and 12.66 KV are taken as the base MVA and base voltage respectively for per-unit representation.

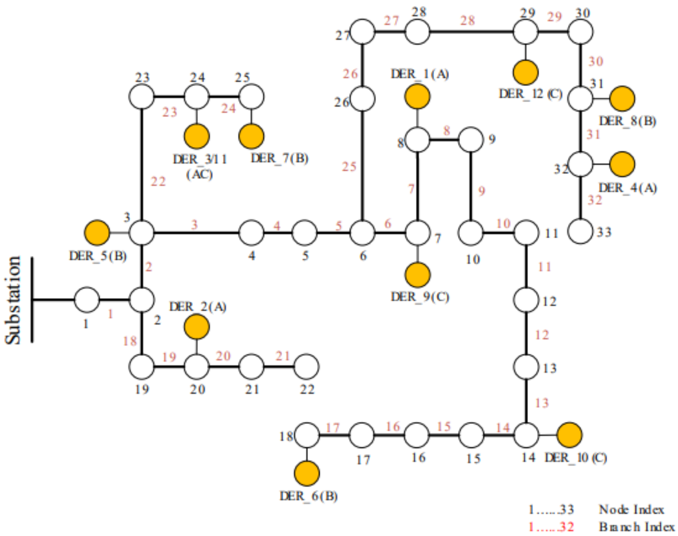

Fig. 3. Modified 33-node Distribution System

Table-I demonstrates a case when the SO requests an increase of DER generation by 400 kW from one distribution feeder. There are 12 single phase DERs placed in different phases and locations of the system. The first column of Table-I represents the DERs with their phase and node location, the second column represents the initial operating points of each DERs, the third column represents the set-points after the optimal re-dispatch problem is solved based on the requested change of power by the SO, and the last column shows the amount of change before and after the re-dispatch. When the loads are considered as ZIP models, their consumption depends on the node voltages which can vary before and after the optimal re-dispatch of DERS.

In the scenario of 400 kW requested change of power at the substation, as re-dispatch of DERs leads to a new system state (i.e., voltages), the total load of the feeder is increased by 11.2 kW and needs to be supplied by the DERs to make up the change in the power provided by the grid. The solution of optimization is fed into the ACPF modelled in OpenDSS, to determine the injected power at the substation, whereas an actual sensor or power measurement devices are installed in reality. As the overall generation from the DERs increases, loss reduces from 149.897 to 128.876 kW. Thus, the total change in active power output of DERs considering the loss and increment in total load demand is 390.66 kW. It can be seen that the power supplied by the grid changes by 400.43 kW. The final absolute percentage error calculated for this scenario is 0.1075% which demonstrates the good accuracy of the linearized optimization model.

Table-II presents an optimal dispatch for an instance when the SO required a negative reference power of 350 kW to down-regulate the frequency. The optimization engine reduces the set-points of most of the DERs whereas DERs at node 32, 18 ,14 and 29 set-points are increased.

The above combination of operating points of DERs provides the minimum loss for this specific case. As the total generation from DERs decreases, the loss of the system as a whole is increased from 134.656 kW to 143.852 kW whereas in this scenario the total demand of the system decreases by 5.1 kW. So, the total reduction in DERs power is by 345.253 kW and the power change in substation is by 349.31 kW.

TABLE-I: OPTIMIZATION SOLUTION FOR 400 KW POWER REQUEST (IEEE 33)

DER(Node-Phase)/Factor	Initial (kW)	Final (kW)	Change (kW)
DER_1 (8-a)	30	70	40
DER_2 (20-a)	15	10	-5
DER_3 (24-a)	50	125.81	75.81
DER_4 (32-a)	40	70	30
DER_5 (3-b)	20	10	-10
DER_6 (18-b)	15	30	15
DER_7 (25-b)	60	115.79	55.79
DER_8 (31-b)	20	51	31
DER_9 (7-c)	40	65	25
DER_10 (14-c)	20	42	22
DER_11 (24-c)	30	126.02	96.02
DER_12 (29-c)	25	40	15
Total Load(MW)	3495.3	3506.5	11.2
Ploss(kW)	149.897	128.876	-21.021
Pgrid(MW)	3280.15	2879.72	-400.43

TABLE-II: OPTIMIZATION SOLUTION FOR -350 KW POWER REQUEST (IEEE 33)

DER(Node-Phase)/Factor	Initial (kW)	Final (kW)	Change (kW)
DER_1 (8-a)	60	56.747	-3.253
DER_2 (20-a)	20	10	-10
DER_3 (24-a)	115	10	-105
DER_4 (32-a)	60	70	10
DER_5 (3-b)	20	10	-10
DER_6 (18-b)	20	30	10
DER_7 (25-b)	120	10	-110
DER_8 (31-b)	45	51	6
DER_9 (7-c)	50	10	-40
DER_10 (14-c)	30	42	12
DER_11 (24-c)	130	10	-120
DER_12 (29-c)	25	40	15
Total Load(MW)	3503.4	3498.3	-5.1
Ploss(kW)	134.656	143.852	9.196
Pgrid(MW)	2943.05	3292.36	349.31

B. *Case Study on the Modified 13-node Test Feeder*

The IEEE 13 node feeder is modified by omitting the line between 650 and 630 including the voltage regulator, the switch between 671 and 692 is assumed to be closed and a 670 node is created in between node 632 and 671 to concentrate a distributed load. Three phase delta load is converted to three single-phase loads by dividing the total load in three equal portions and is assigned to three respective nodes. This approximation is suitable for the power flow model when each phase is decoupled and analysed separately. All data related to feeder topology, spot loads, line length, line impedances are taken from [15].

Table-III represents the optimal dispatch of DERs participating for frequency regulation problem. For this scenario, SO requests a positive reference power of 400 kW and the optimizer requires two iterations to dispatch the requested amount as 4.97 kW power is deficit from the first iteration. In this case also, because of the ZIP loads the total amount load consumption increases from 3459.8 kW to 3461.4 kW. When the solution of optimal dispatch obtained using linearized optimal power flow is tested using ACPF, the solution demonstrates the power at the substation change by 395.02 kW. The absolute percentage error is 1.244%. Table-IV represents the result of optimal power flow for corrective action, and it can be observed that the starting operating point of second layer of optimization is the final set-points from the first layer of optimization. Furthermore, the operating point of DER only installed at phase c of node 670 whose output power changes from 224.70 kW to 229.65 kW as the amount that needs to be corrected is only 4.97 kW. It can also be seen that the power coming from the grid changes by 4.965 kW and there is small reduction in the loss of the system to compensate the mismatch.

Table-V and Table-VI represent an example when the SO requests to decrease the generation of DERs by 700 kW to reduce the frequency. Such scenario in the power system can be observed when the generation exceeds the total demand of the system. In this case as well, the optimizer engine dispatches the SO requested power after the second iteration. As in the first iteration, the power supplied from the grid is not exactly increased by 700 kW but by 697.225 kW which indicates a deficit of 2.7748 kW for which the second iteration of optimization is required. During the second iteration of optimization, only DER_9 set point is changed from 194.94 kW to 192.27 kW to balance the mismatch. Loss reduces by only 0.09 kW as the change in the total output of DER is only 2.67 kW. Aggregation of both the change in loss and the change in total output power of DERs compensate the deficit of 2.77 kW observed in the first iteration.

TABLE-III: FIRST ITERATION OPTIMIZATION SOLUTION FOR 400 KW POWER REQUEST (IEEE 13)

DER (Node-Phase)/Factors	Initial (kW)	Final (kW)	Change (kW)
DER_1 (670-a)	100	168.04	68.04
DER_2 (670-b)	80	80	0
DER_3 (670-c)	100	224.70	124.70
DER_4 (633-a)	50	30	-20
DER_5 (633-b)	30	10	-20
DER_6 (633-c)	40	30	-10
DER_7 (675-a)	125	250	125
DER_8 (675-b)	30	50	20
DER_9 (675-c)	100	200	100
Total Load(kW)	3459.8	3461.4	1.6
Ploss(kW)	39.41	30.54	-8.87
Pgrid(kW)	2844.28	2449.26	-395.02

TABLE-IV: SECOND ITERATION OPTIMIZATION SOLUTION FOR 400 KW POWER REQUEST (IEEE 13)

DER (Node-Phase)/Factors	Initial (kW)	Final (kW)	Change (kW)
DER_1 (670-a)	168.04	168.04	0
DER_2 (670-b)	80	80	0
DER_3 (670-c)	224.70	229.65	4.95
DER_4 (633-a)	30	30	0
DER_5 (633-b)	10	10	0
DER_6 (633-c)	30	30	0
DER_7 (675-a)	250	250	0
DER_8 (675-b)	50	50	0
DER_9 (675-c)	200	200	0
Total Load(kW)	3461.4	3461.4	0
Ploss(kW)	30.54	30.528	-0.012
Pgrid(kW)	2449.26	2444.295	-4.965

TABLE-V: FIRST ITERATION OPTIMIZATION SOLUTION FOR -700 KW POWER REQUEST (IEEE 13)

DER (Node-Phase)/Factors	Initial (kW)	Final (kW)	Change (kW)
DER_1 (670-a)	300	100	-200
DER_2 (670-b)	150	80	-70
DER_3 (670-c)	300	100	-200
DER_4 (633-a)	100	30	-70
DER_5 (633-b)	50	10	-40
DER_6 (633-c)	100	30	-70
DER_7 (675-a)	250	250	0
DER_8 (675-b)	50	10	-40
DER_9 (675-c)	200	194.95	-5.05
Total Load(kW)	3459.9	3458.5	-1.4
Ploss(kW)	27.79	31.2	3.4
Pgrid(kW)	1988.83	2686.055	697.225

TABLE-VI: SECOND ITERATION OPTIMIZATION SOLUTION FOR -700 KW POWER REQUEST (IEEE 13)

DER (Node-Phase)/Factors	Initial (kW)	Final (kW)	Change (kW)
DER_1 (670-a)	100	100	0
DER_2 (670-b)	80	80	0
DER_3 (670-c)	100	100	0
DER_4 (633-a)	30	30	0
DER_5 (633-b)	10	10	0
DER_6 (633-c)	30	30	0
DER_7 (675-a)	250	250	0
DER_8 (675-b)	10	10	0
DER_9 (675-c)	194.94	192.27	-2.67
Total Load(kW)	3458.5	3458.5	0
Ploss(kW)	31.2	31.29	0.09
Pgrid(kW)	2686.055	2688.815	2.76

V. Conclusion

This paper has proposed an approach for SFR through optimal re-dispatch of distributed energy resources (DERs). As the activation time-frame requirement for participating DERs for SFR is within few seconds to minutes, non-linear AC power flow model is linearized for faster computation of optimal set-points of DERs. The request of SOs for regulating the frequency is fulfilled through the formulation of an iterative optimization problem with SO's command as one of the constraints and network loss minimization as the objective function. The effectiveness of the proposed approach is validated using unbalanced modified 33 and IEEE 13-node distribution systems with embedded DERs and ZIP load models. The results show that the proposed approach can optimally re-dispatch the DERs to fulfil the request of SOs for better SFR with an acceptable accuracy and computation time.

Acknowledgement

This paper is based upon work supported by the U.S. Department of Energy's Office of Energy Efficiency and Renewable Energy (EERE) under the Solar Energy Technologies Office Award Number DE-EE0009022.

BIBLIOGRAPHY

[1] S. C. Ross, G. Vuylsteke, and J. L. Mathieu, “Effects of load-based frequency regulation on distribution network operation,” *IEEE Transactions on Power Systems*, vol. 34, no. 2, pp. 1569–1578, 2019.

[2] C. R. Shapiro, P. Bauweraerts, J. Meyers, C. Meneveau, and D. F. Gayme, “Model-based receding horizon control of wind farms for secondary frequency regulation,” *Wind Energy*, vol. 20, no. 7, pp. 1261– 1275, 2017.

[3] S. Boersma, B. Doekemeijer, S. Siniscalchi-Minna, and J. van Wingerden, “A constrained wind farm controller providing secondary frequency regulation: An les study,” *Renewable energy*, vol. 134, pp. 639–652, 2019.

[4] A. Zeh, M. Mueller, H. C. Hesse, A. Jossen, and R. Witzmann, “Operating a multitasking stationary battery storage system for providing secondary control reserve on low-voltage level,” in *International ETG Congress 2015; Die Energiewende-Blueprints for the new energy age*. VDE, 2015, pp. 1–8.

[5] M. Gheisarnejad, M.-H. Khooban, and T. Dragicevi ˇ e, “The future´ 5g network-based secondary load frequency control in shipboard microgrids,” *IEEE Journal of Emerging and Selected Topics in Power Electronics*, vol. 8, no. 1, pp. 836–844, 2019.

[6] J. Tan and Y. Zhang, “Coordinated control strategy of a battery energy storage system to support a wind power plant providing multi-timescale frequency ancillary services,” *IEEE Transactions on Sustainable Energy*, vol. 8, no. 3, pp. 1140–1153, 2017.

[7] E. Rebello, D. Watson, and M. Rodgers, “Performance analysis of a 10-MW wind farm in providing secondary frequency regulation: Experimental aspects,” *IEEE Transactions on Power Systems*, vol. 34, no. 4, pp. 3090–3097, 2019.

[8] M. D. Galus, S. Koch, and G. Andersson, “Provision of load frequency control by PHEVs, controllable loads, and a cogeneration unit,” *IEEE Trans. Ind. Electron.*, vol. 58, no. 10, pp. 4568–4582, 2011.

[9] T. Masuta and A. Yokoyama, “Supplementary load frequency control by use of a number of both electric vehicles and heat pump water heaters,” *IEEE Transactions on smart grid*, vol. 3, no. 3, pp. 1253–1262, 2012.

[10] X. Chen, Q. Hu, Q. Shi, X. Quan, Z. Wu, and F. Li, “Residential HVAC aggregation based on risk-averse multi-armed bandit learning for secondary frequency regulation,” *Journal of Modern Power Systems and Clean Energy*, vol. 8, no. 6, pp. 1160–1167, 2020.

[11] P. Li, Z. Tan, Y. Zhou, C. Li, R. Li, and X. Qi, “Secondary frequency regulation strategy with fuzzy logic method and self-adaptive modification of state of charge,” *IEEE Access*, vol. 6, pp. 43575–43585, 2018.

[12] M. Baran and F. Wu, “Optimal sizing of capacitors placed on a radial distribution system,” *IEEE Transactions on Power Delivery*, vol. 4, no. 1, pp. 735–743, 1989.

[13] C. Zhang, Y. Xu, Z. Dong, and J. Ravishankar, “Three-stage robust inverter-based voltage/var control for distribution networks with highlevel PV,” *IEEE Trans. Smart Grid*, vol. 10, no. 1, pp. 782–793, 2019.

[14] J. Zhang, M. Cui, B. Li, H. Fang, and Y. He, “Fast solving method based on linearized equations of branch power flow for coordinated charging of EVs (EVCC),” *IEEE Transactions on Vehicular Technology*, vol. 68, no. 5, pp. 4404–4418, 2019.

[15] W. Kersting, “Radial distribution test feeders,” in *2001 IEEE Power Engineering Society Winter Meeting. Conference Proceedings (Cat.No.01CH37194)*, vol. 2, 2001, pp. 908–912 vol.2